Anisotropy and Petrophysics of a Gas Reservoir in a Horizontal Well with a High Angle Pilot Well, Burgos Basin, Mexico*

Hugo Avalos Torres[1], Heriberto Córdova Aguayo[1], Manuel Morales Leal[1], José Bernal Monjaras[1], Eric Pacheco P.[2], Erik Martínez S.[2], and Gelmunt Escamilla V.[2]

Search and Discovery Article #40525 (2010)
Posted April 30, 2010

*Adapted from extended abstract prepared for poster presentation at AAPG International Conference and Exhibition, Rio de Janeiro, Brazil, November 15-18, 2009

[1]PEMEX North Region, AIB México (havalost@pep.pemex.com) .
[2]Halliburton de México

Abstract

The present work shows two important concepts in gas reservoir description, anisotropy and petrophysica; properties; this study was performed of a reservoir drilled by the well Bayo-35H which is a horizontal well with a high angle pilot well, the Bayo-35. The Bayo field is located in Burgos basin oriental area.

The study starts with the concern of the integration of conventional core data and special and conventional well logs; obtained in open hole, with the objective to calibrate, detail, and analyze with better precision the anisotropic and petrophysical characteristics, also to define the reservoir potential qualitatively and quantitatively.

This reservoir has a net thickness between 25 and 70 meters, composed of siliciclastic sediments from the Eocene in the Jackson Medium (Middle) Formation (Ejm). These sands show excellent porosity "ø" (between 14 and 35 %) and excellent permeability "k" (between 4 mDarcy to 3.5 Darcy) obtained from core data.

Anisotropic and petrophysical properties and types of rock are described in this article, such as: anisotropy, heterogeneity, index of reservoir quality, rock types, flow units, R35 and FZI (by means of Windland plot and modified Lorenz), salinity (NaCl) and Rw, electrical properties, and mineralogy of this producing sand. Conclusions have been based on the study of cores(conventional and sidewall cores), cross-plots, petrographic and scanning electron microscope (SEM) images, and interpretation and evaluation of special logs.

This reservoir has produced gas and condensate, at a rate of 1 to 5 mmscf; the bottom hole flowing pressure is from 650 to 750 psi. Actual production history shows an accumulated production of 4 Bscf.

Introduction

In the last years, the Burgos Basin has become one of the most important dry gas producing basins in Mexico. The Activo Integral Burgos (AIB) has added important gas potential reserves; it has been possible, thanks to multidisciplinary team and carefully planned workflows. An example of this type of study described here is from one of the basin oriental area's gas reservoirs.

Integration and detail about the petrophysical and anisotropic reservoir characteristics have a direct implication in calculating reserves; this information is also important for drilling engineering and well completion. For this reason, reservoir analysis and evaluation have become two important properties to considering in making decisions about completions and potential economic evaluation of a particular area.

Location

Tertiary Burgos basin is located in the western Gulf of Mexico region in northeastern Mexico, mainly in Tamaulipas and Nuevo León states. Study area is located on eastern Burgos Basin close to Reynosa City (Figure 1).

Objectives

This work is intended to cover the following objectives:
Characterize the reservoir Ejm7, beginning with the data integration obtained during the drilling and completion of the B-35H well.
Determine anisotropy and petrophysics characteristics.
determine the stresses magnitude, formation heterogeneous characteristics, mineralogy, grain size, NaCl (Rw).
Perform a petrophysics subdivision through rock types and determination of flow units.

Background

The Bayo field was discovered in 2004, with the B-1 wildcat well. This well was a gas producer at 790 m and 900 m zones in Eocene Jackson Middle Formation. It is appropriate to mention that there was already exploratory well Numerator-1, a producer at 710 meters in the vicinity of the field. The field currently consists of 16 producer wells. Bayo-6 well began the development of this field in 2006, discovering producing sand between 650 and 700 meters.

Reservoir net thickness has range from 50 to 70 meters, in Eocene siliciclastic sediments in Jackson Middle formation. This reservoir has excellent porosity (ø range 15 to 35 %) and permeability (k ranges from 0.4 mD to 4 D), provided by cores.

A static 3-D model was developed, in order to define exactly where the pilot well was to be drilled and ensure success of drilling horizontal well (Figure 2). The pilot well is used to know: where the productive reservoirs are, support the static model, recover conventional core,

develop facies model from open hole logs, and compare it with the static model. This correlation had a 90% success.

Compared with the pilot well, the model results were satisfactory; for the model projected a depth of 716 meters TVD (vertical depth) to the the top of the objective, and the objective is at 718 meters TVD--only 2 meters of difference. With this result, the model could be trusted to guide the horizontal drilling of well B-35 H.

Garrido et al. (2009) confirmed the data obtained from the pilot well, and by using the static model, proceeded to generate the surface of the objective (with the value of the dip in the area of interest), making it possible to define a trajectory for the horizontal well segment. The average dip is 3°; the average navigation angle was 88.8°; azimuth was 130° at 723 meters TVD. Type of completion was expandable liner medium mesh screen from 1030 to 1372 MD, with an approximate length of 300 meters.

Development

Sedimentology: Ejm7 Reservoir As a Rock

The Ejm7 (Figure 3) pay is the most important sand, from the point of view of the Bayo field gas production. The data from the conventional and sidewall cores permit characterization of the reservoir according to classification, texture, particle size, composition, and mineralogy. These parameters, calibrated to the petrophysical features, are considered essential in interpretation and evaluation of the reservoir.

The core showed mainly one bituminous sand, with two shades of grey (light and dark), of quartz and lithic fragments, generally fine- to very fine-grained, well sorted, subangular, subspherical, poorly consolidated, calcareous cement. The sand contains bitumen, disseminated pyrite, mica, some glauconitic grains, and common undetermined fossils. Two intervals characterized within the core, are as follows:

Interval: 946 to 948 Meters

In this interval the sandstones with sizes ranging from very fine at the top to medium at the bottom, with a grey color tinged with green, interstratified in a chaotic way with light grey shell fragment (coquina) and fossiliferous shaly sands, slightly conglomeratic (top of Figure 4). Mud and sandstone fragments are present within the conglomeratic and coquina beds. as well. The majority of fossil fragments are big mollusks (oysters); these fragments are randomly oriented. Some portions of the intervals are clearly bioturbated, *Ophiomorpha* holes can be identified. The base of the interval is very irregular and indistinct, with *Glossifungites*.

The complex and distorted stratification, the big fossil fragments, the shaly fragments, and the large size of other clasts suggest fast and periodic depositional rates and local erosion. The abundance of big oysters points out that they thrived in the general environment, as observed in Figure 5.

The indistinct area in core of *Glossifungites* (with *Ophiomorpha* holes) does not suggest an apparent change in the environment. This area could have been formed out of erosion generated by a tidal channel cutting through lagoon sediments on tidal flat. The *Glossifungites,* developed in firm sediment, are associated with late erosion events, such as coastal erosion processes or the migration of a tidal channel (Core Lab, 2008).

Given the current data set, the most plausible interpretation is that this interval represents filled tidal channel. The oysters came from a nearby lagoon (visible traces in Figure 5). Another less plausible possibility is that this interval represents a period of transgression and coastal or deltaic erosion.

Interval: 948 to 955 Meters

In this interval sand ranges in grain size from very fine to fine and in color from greenish-grey to light grey. The intervals with bioturbation contain more clay and exhibit a lightly darker grey color; similarly, two intervals cemented with chlorite can be differentiated between 951.65 and 952.66 meters and between 953.00 and 953.25 meters (Figure 6). Big *Ophiomorpha* (diameter: 2-4 cm) are present along the entire interval, but they are more frequent towards the top. The holes from bioturbation, which appear from the top of the interval down to 948.42 meters, contain seashells from the upper bed (as described in the previous interval), suggesting that this upper contact could have served as *Glossifungites* surface (firmground). Some shaly clast-scarred rock fragments are identified at 949.90, 952.38, and 954.68 meters; a big sea shell fragment is present at 951.77 meters, as well.

The grain size in this interval (upper fine sand to fine sand) and the shaly-scarred rock fragments point to a high energy depositional environment.

The absence of preserved sedimentary structures suggests two possibilities:

1. Deposition occurred at a very fast pace, and the sediment drainage homogenized the sediments.
2. Bioturbation was more extensive than what is observed in the core, due to the absence of dissimilar sediment.

Ophiomorpha is a clear indicator of the marine influence. The *Ophiomorpha* prefers high- energy environments.

Sedimentary Environment

The facies analysis (electrofacies), achieved with the existing well logs, agrees in general with regional interpretations that this reservoir is part of a group of reservoirs that are high-energy clastic sediments (deltaic systems, complex coastal barriers); correspondingly, some of these reservoirs show clean sands that can be associated with barrier deposit or coastal barriers. This information, altogether with disturbed strata and sea-shell fragments in the top interval of the core, favors the interpretation corresponding to a littoral barrier/estuary deposition.

It is possible that interval could have been deposited as a distributary mouth-bar, given that the disturbed, chaotic sediments in the upper part of it were part of an abandonment and associated reworking on the delta (Figure 7).

Classification

Based on the composition and description, this sandstone is classified as "feldspathic litharenite" (Folk, 1974), as shown in Figure 8.

Petrography and Scanning Electron Microscopy

The photomicrographs (Figures 9 and 10) and the images from the scanning electron microscope (Figures 11 and 12) of core samples allow us to identify the cement, type, distribution, and characteristics of the constituents, including the clays (illite, smectite, and chlorite). Gunter and Viro (2006) state that this type of study allows one to get an idea of the pore-throat sizes and configuration, the cement type that causes obstruction, in some cases, and how one grain can affect another.

Figures 9, 10, 11, and 12 show common macro-pores (blue); primary porosity (intergranular) and secondary porosity (intragranular); it can also be observed that the pores are well connected; also there is a fair amount of secondary pores (grain-size pores), which have diminished the effects of mechanical compaction.

This fine-grained sandstone has plenty of visible pores, the majority of which are primary pores.

As described earlier, the rock composition is quartz, some feldspar, and lithic fragments. The sorting is good, although there are grains of different sizes; grains are subangular and subrounded. Please note the big foraminifer (For) in Figure. 9. In the view are: quartz (C), plagioclase (P), limestone fragments (FCc), grains replaced by ferrous calcite (Fcalg), grains replaced by shale (ar_g), grains replaced by ferrous dolomite (Fdolg), and igneous rock fragments (Fi). As this rock has good permeability (k), hydraulic fracturing will not be necessary.

In this sandstone, with fine grains and good sorting, the intergranular pores are open and seem to have a good interconnection; the compaction appears to be light. The patches of analcime cement in Figure 10 are less frequent. The grains shown in the enlarged image (Figure 10) are quartz (C), limestone fragments (FCc), grains replaced by ferrous calcite (Fcalg) and igneous rock fragments (Fi).The analcime cement is also shown (ana).

In the fine-grained sandstone shown in Figure 11, the intergranular pores are abundant and have good interconnection. Some traces of potassic feldspar overgrowth and ferrous calcite cement are observed (Fcal). In the enlarged image (Figure 11) small quartz overgrowths (sdc) are present on some grains.

Salinity (NaCl)

The Ejm7 reservoir has only produced dry gas, no connate water has been recovered, and therefore the water resistivity (Rw) has been calculated using salinity (NaCl) of 9000 ppm from a sample recovered from the well Bayo-6 lin the Ejm 6 reservoir. This reservoir is located between 100 and 150 meters away in the vertical direction. The Rw used is: 0.514 at 35°C.

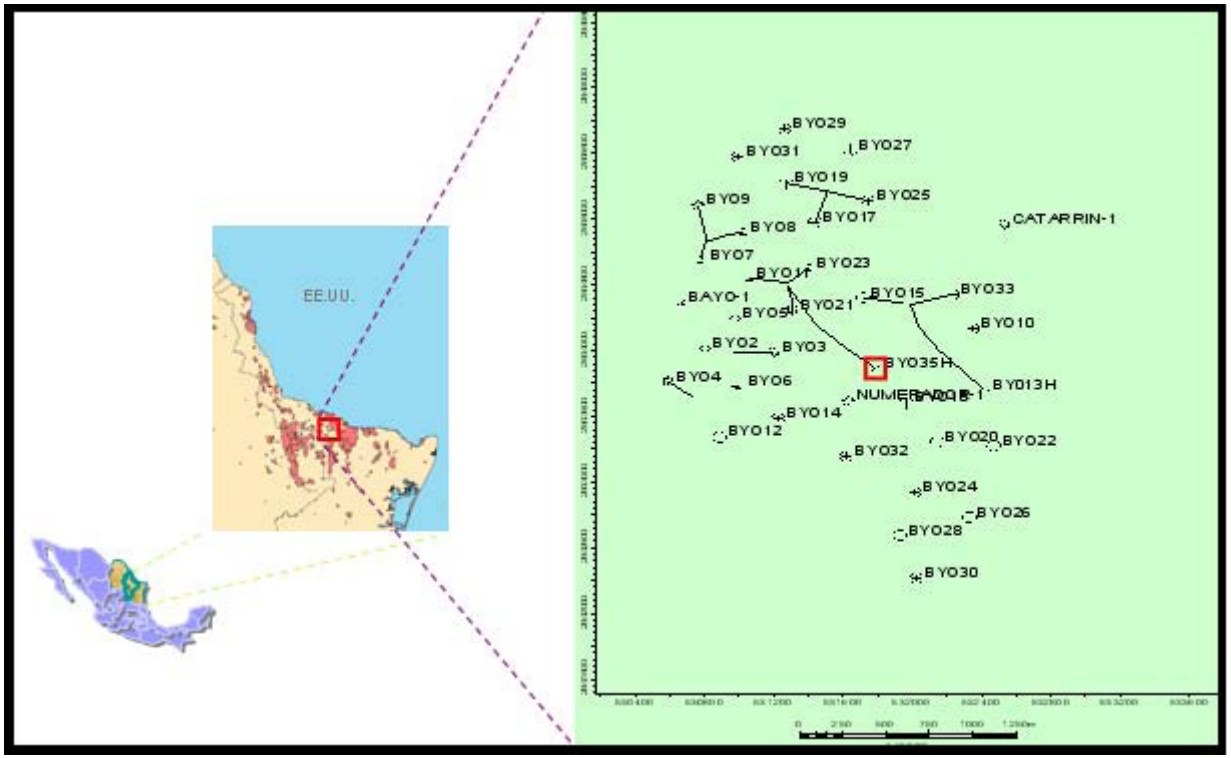

Figure 1. The figure shows study area, close to Reynosa city. The red square find B-35H well, on this place was recovered a conventional core. 1

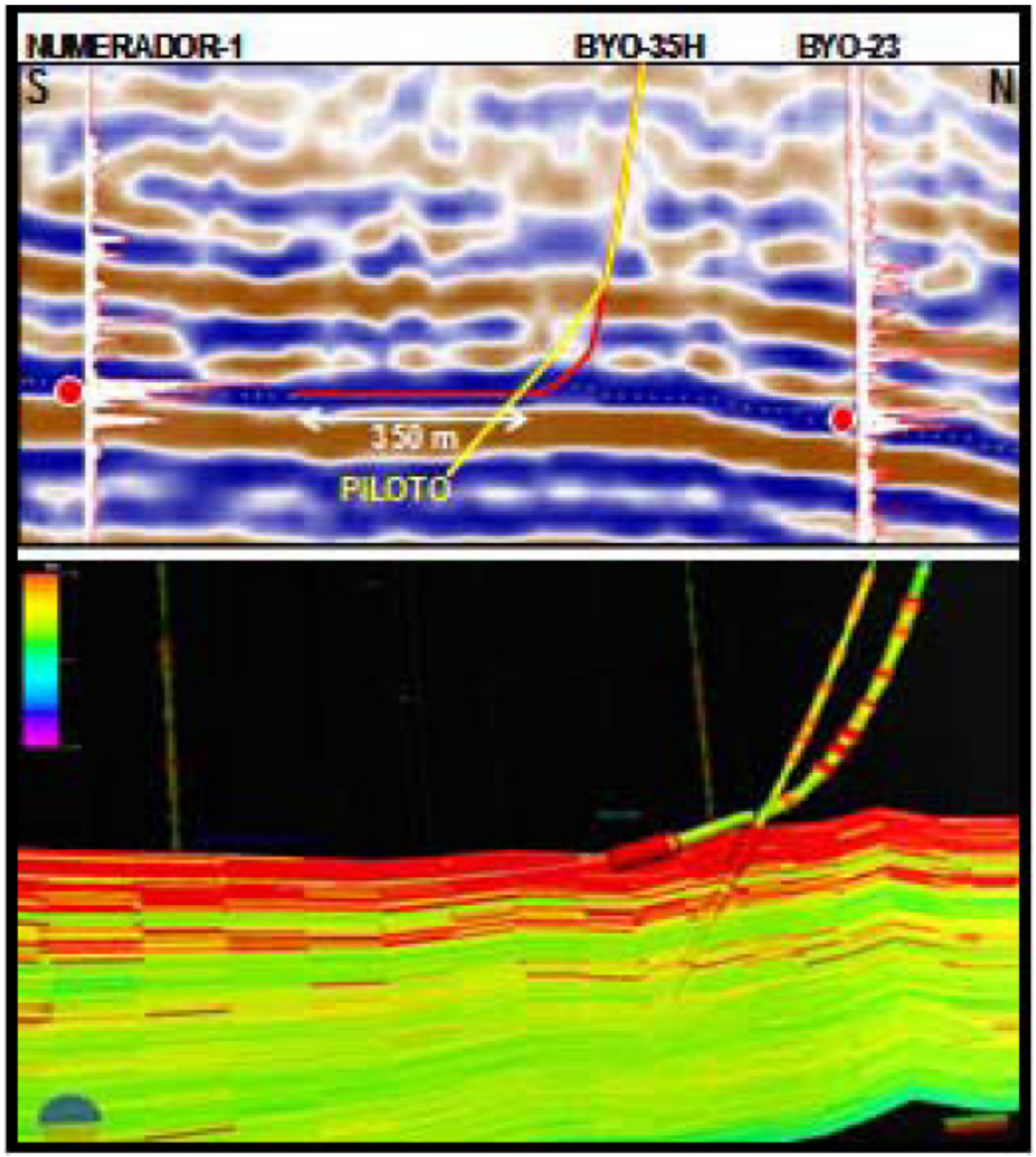

Figure 2. Upper: Seismic section between Numerador-1, B-35H, and B-23, showing that the pilot and horizontal wells are located favorabley with respect to the seismic reflector representing the reservoir. Lower image: static 3D model with the same representation of the wells (Garrido et al., 2009).

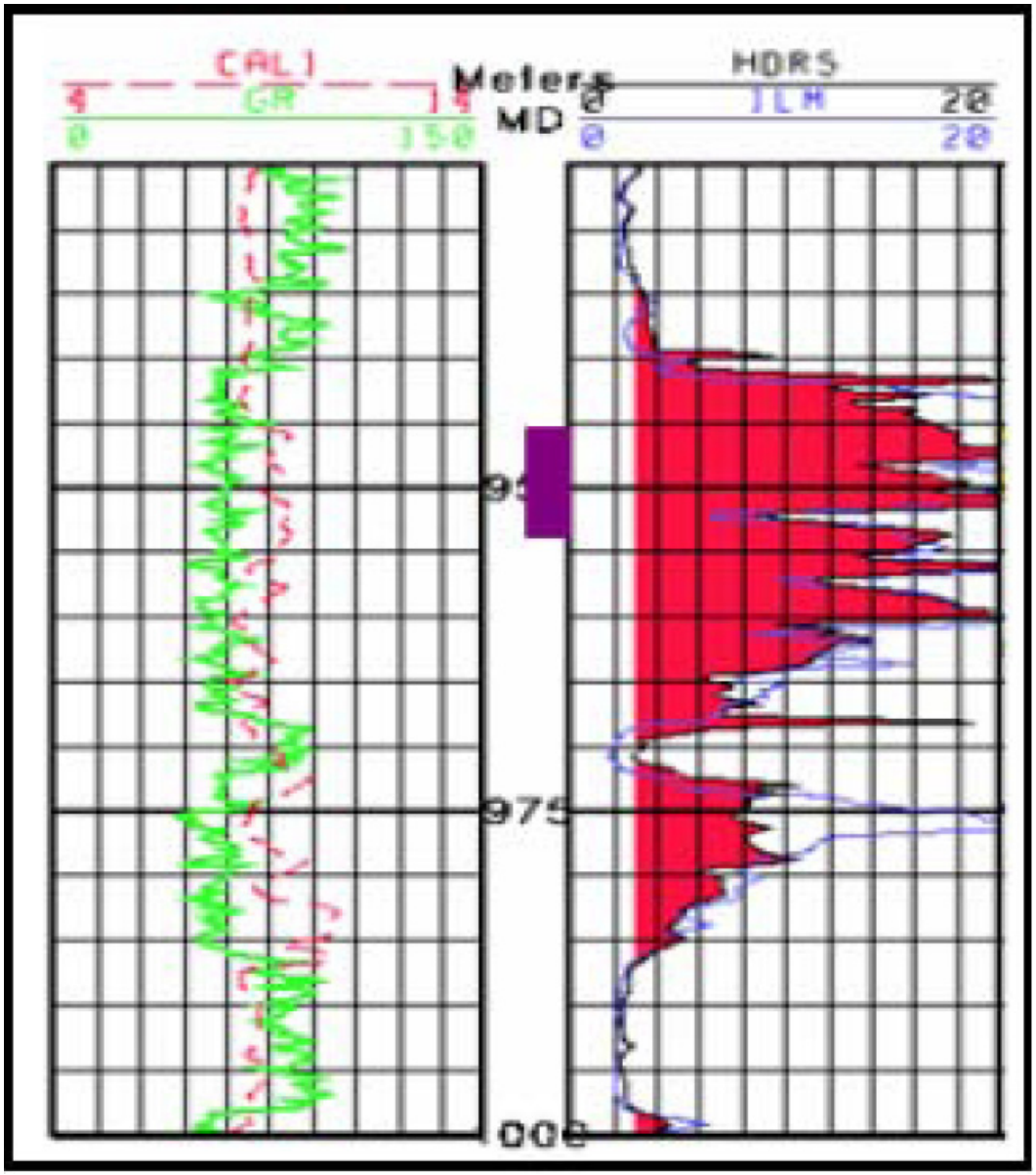

Figure 3. Gamma ray and resistivity curves responses for Ejm7, with position of where conventional core was recovered in B-35H. In Numerador-1 and B-33, sidewall cores were taken in this reservoir.

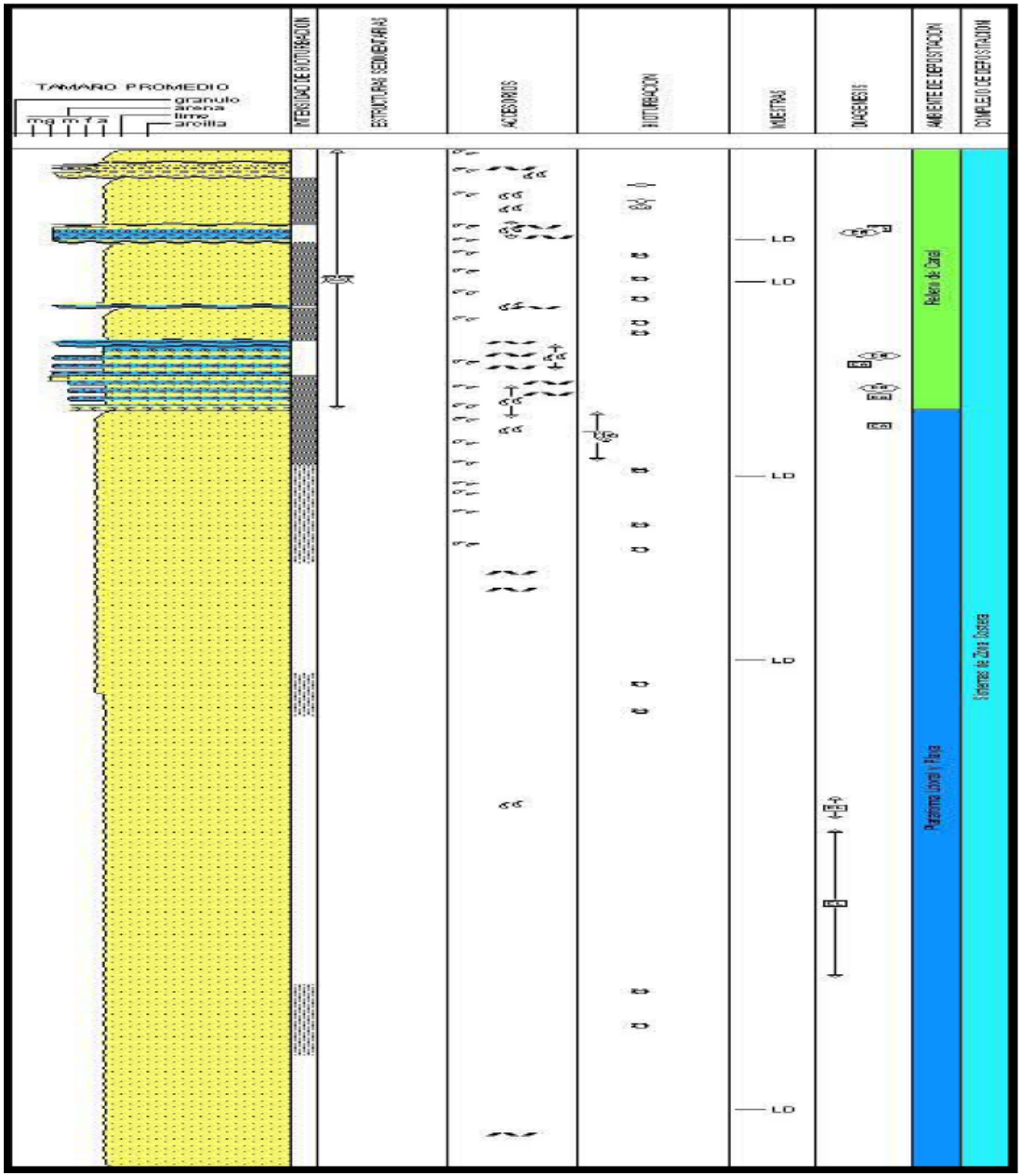

Figure 4. Lithologic log of conventional core in the reservoir Ejm7

Figure 5. Core photograph of interval 946 to 948 m, in B-35H. Note color, texture, and large fossil fragments.

Figure 6. Core interval of 952 to 954 m inB-35H. Note color, texture, and rock quality.

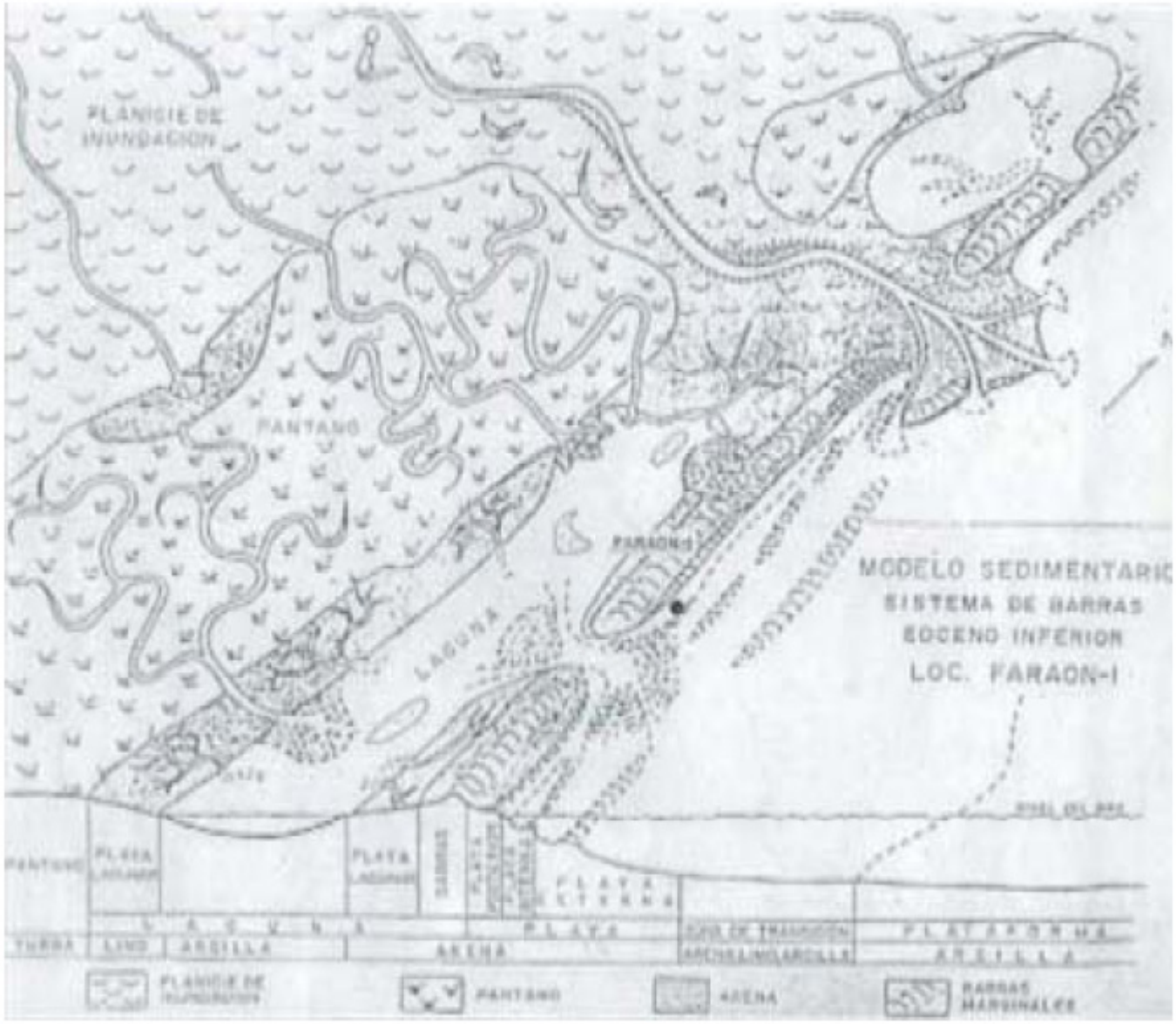

Figure 7. Hypothetical diagrammatic model of a barrier system in deltaic environment dominated by waves. Highlighted area suggests area of the core of the reservoir.

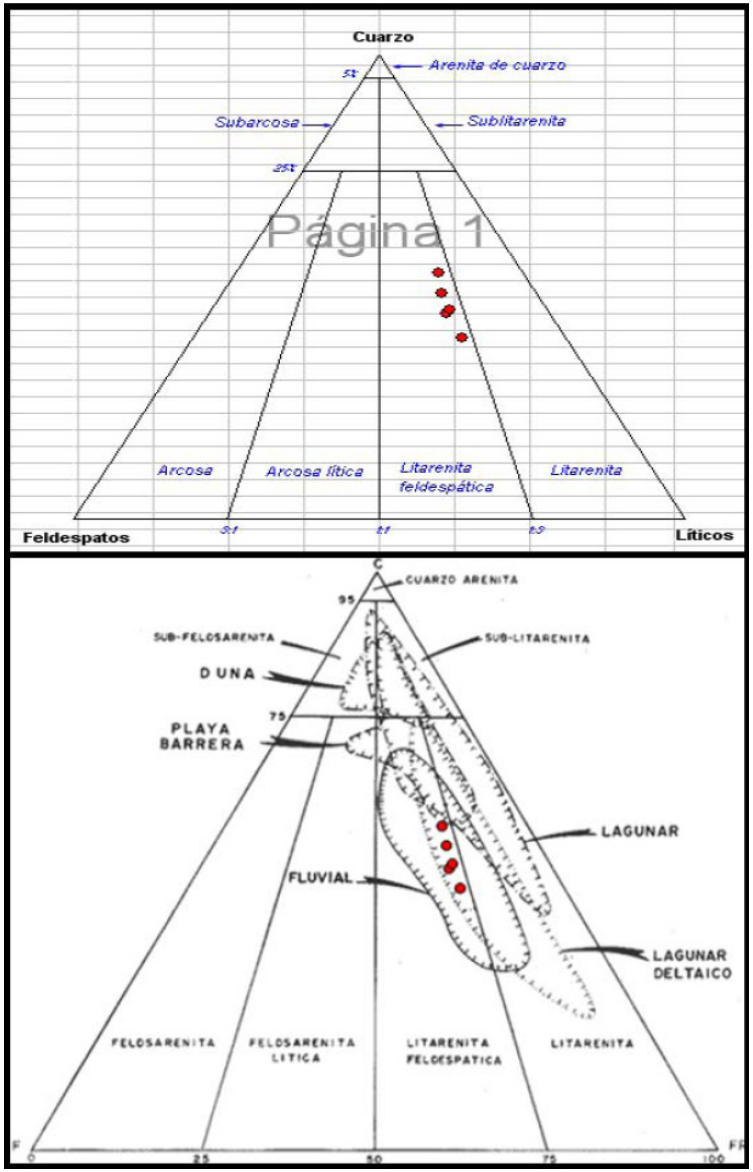

Figure 8. Upper: Based on the classification of Folk (1974), the sandstone is a feldspathic litharenite. Lower: Classification used to estimate sedimentary environment, based on grain size, showing reservoir corresponds to various environments (fluvial, lagoonal, deltaic) (Carranza-Edwards, 1980).

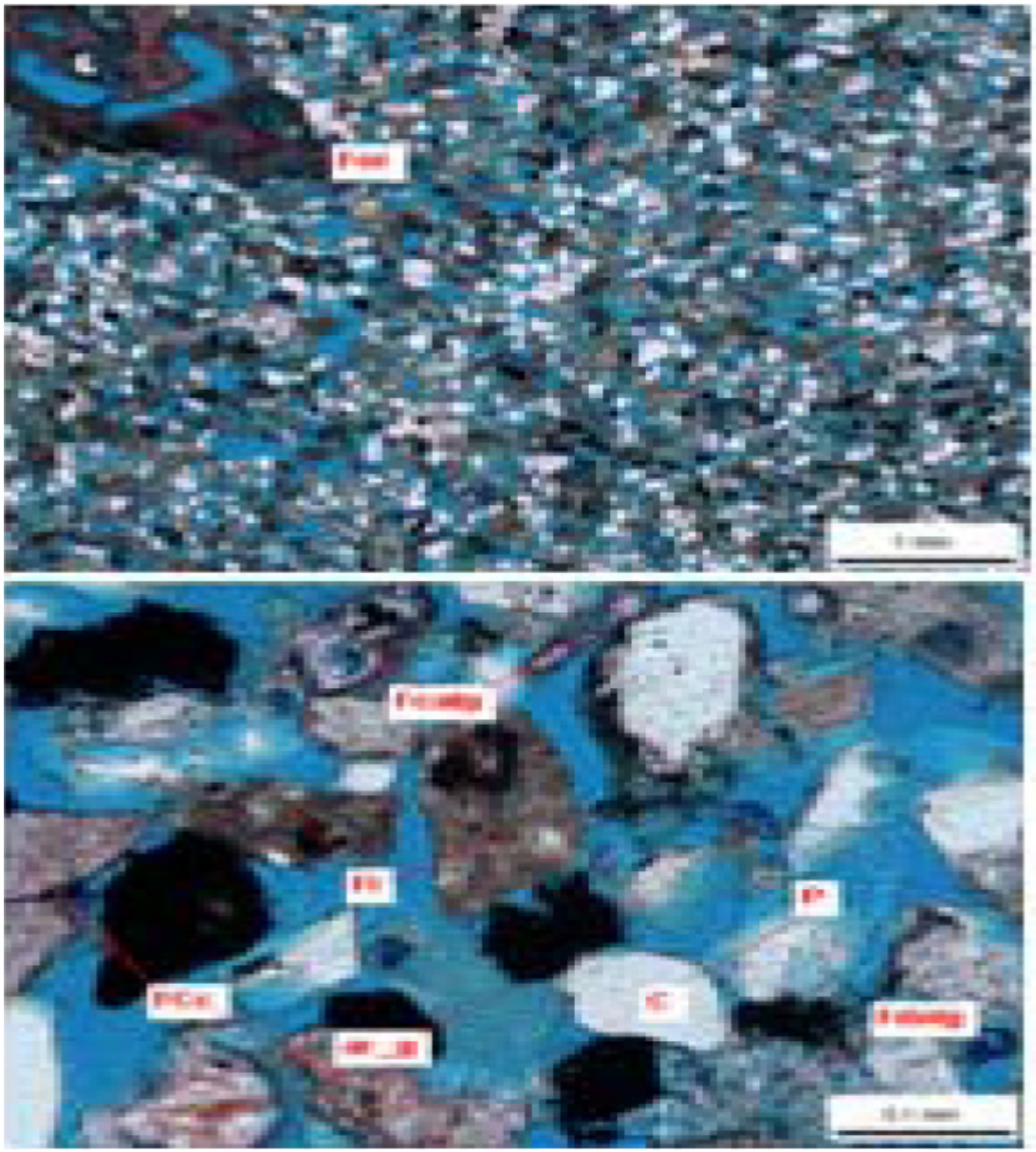

Figure 9. Photomicrographs from conventional core at depth of 947.16 m, sandstone has 31 % porosity (represented by the blue resin) (ø =31 %, k = 2800 mD or 2.8 D) (Core Lab, 2008).

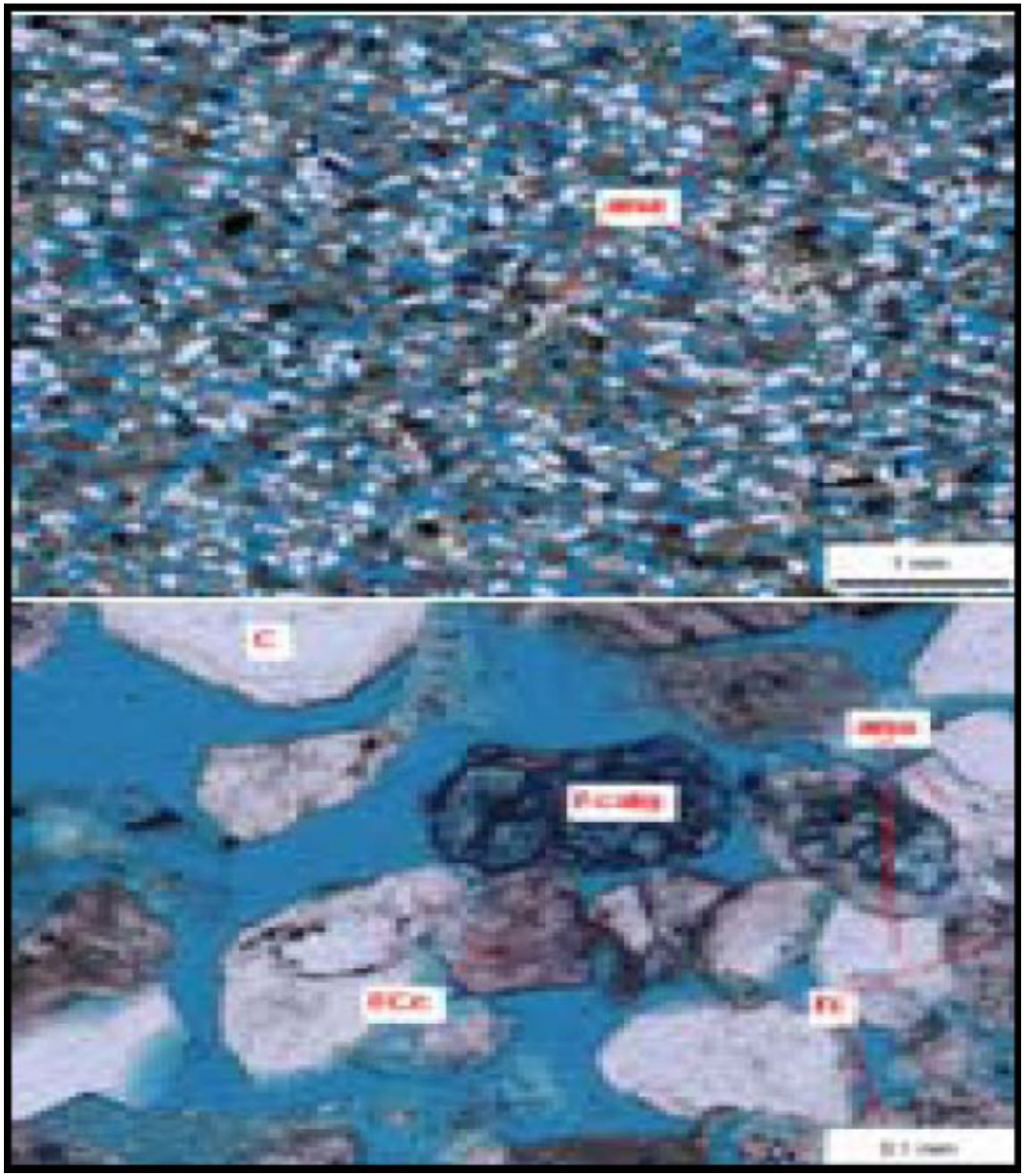

Figure 10. Photomicrographs from the conventional core at a depth of 950.54m. The porosity (blue resin) is 34% (ø =34 %, k = 2902 mD or 2.9 D) (Core Lab, 2008).

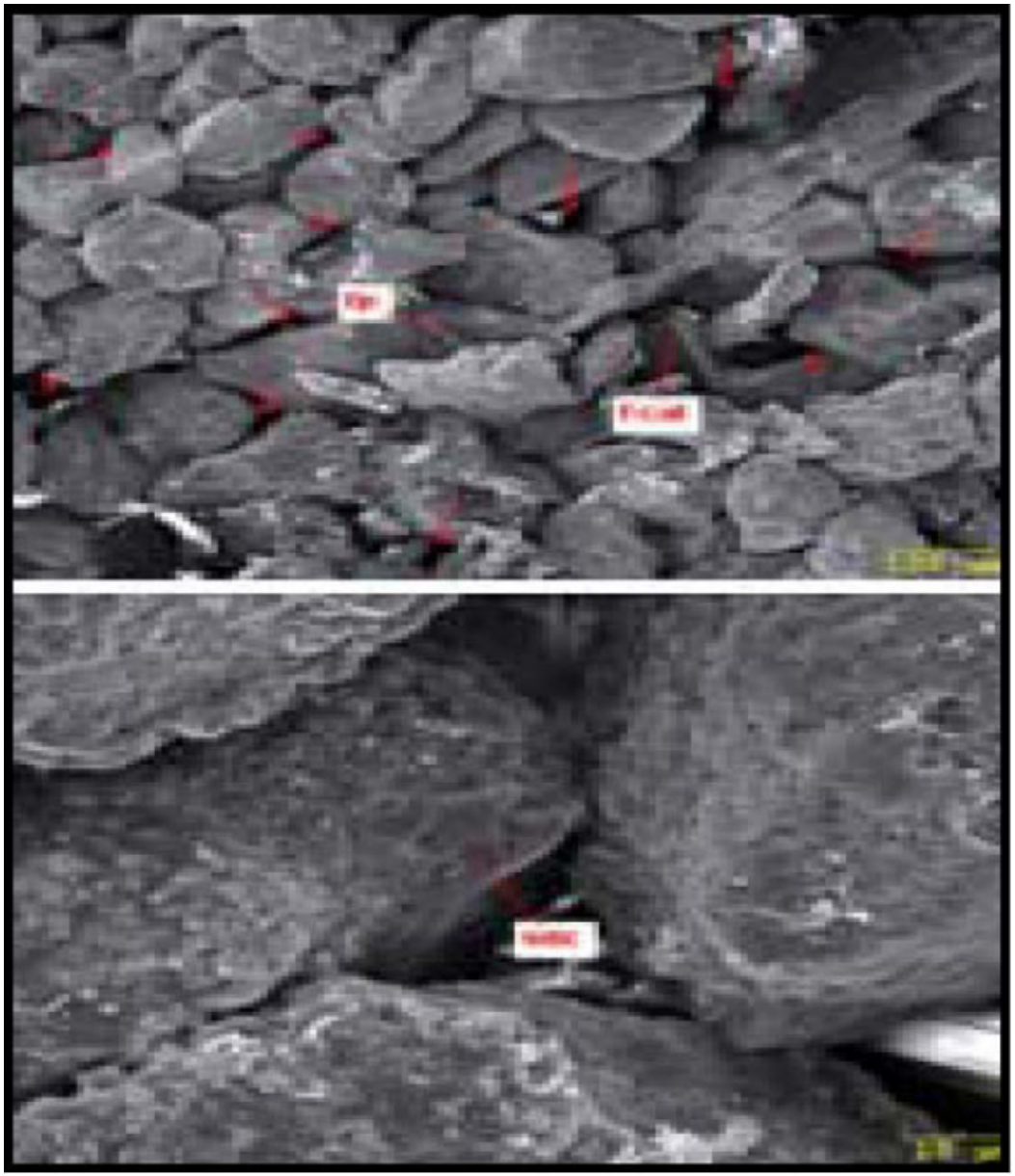

Figure 11. SEM photomicrographs from a depth of 948.88 m. Porosity is 32% (ø = 32 %, k = 2.3 D). The upper image shows the texture and fabric. Lower image shows the sizes of pore throats and grain contacts (Core Lab, 2008).

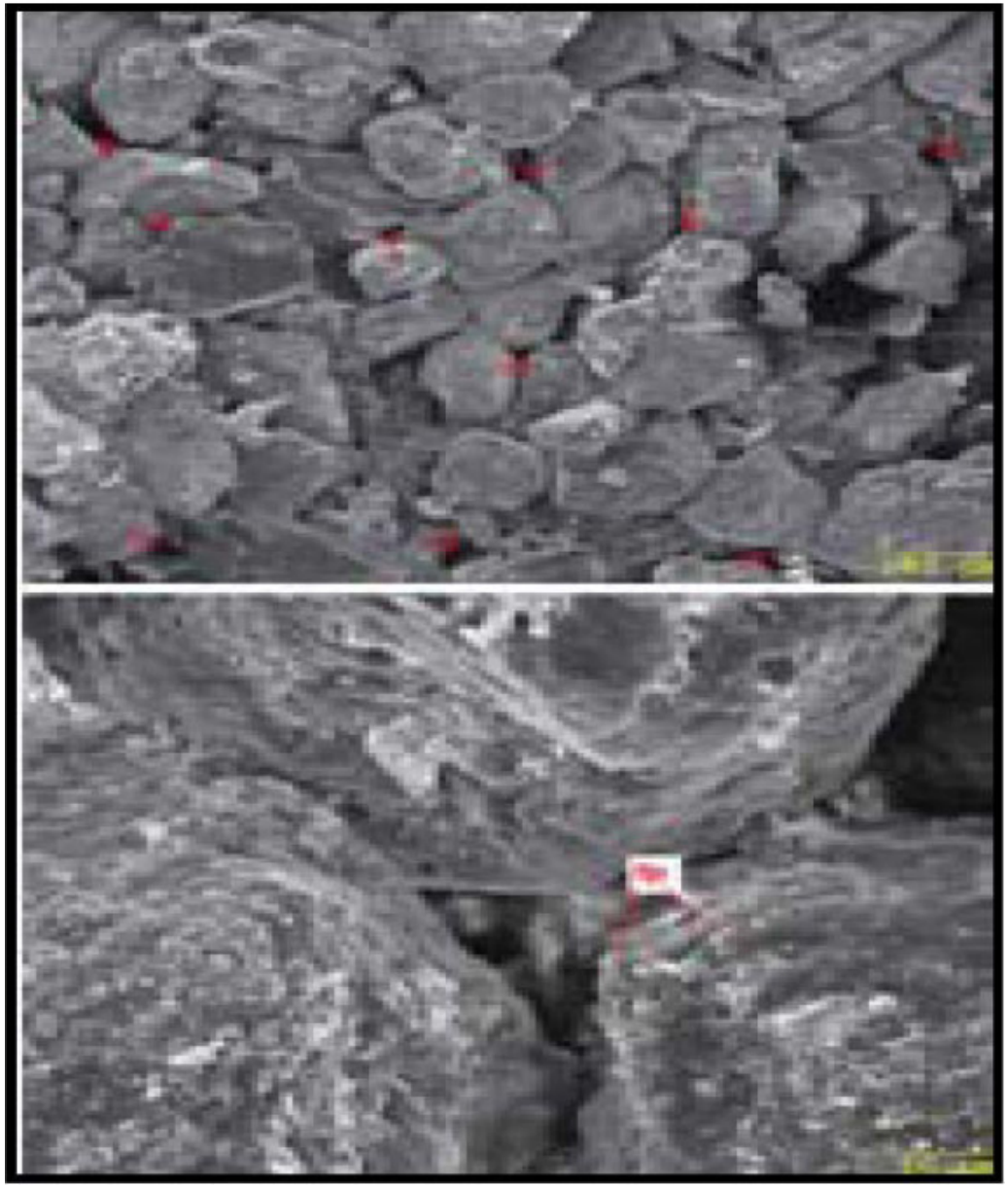

Figure 12. SEM photomicrographs of sample from a depth of 950.54 m. The upper image shows the texture and fabric. Lower image shows the pore-throat sizes and grain contacts (Core Lab, 2008).

Rock Types and Flow Units

To be able to define the flow units, types of rocks and the sizes of pore throats, it is necessary to rely on the data from the conventional core or sidewall cores, for they allow one to calibrate the computed curves (Φ, Sw, k) resulting from the conventional electric logs during the evaluation. The quality of the input data will provide more reliable outputs that will allow development of a better reservoir characterization. Figure 13 is a porosity-permeability plot from the plugs obtained from the conventional core; these hard data were used to calibrate the conventional logs and the computed curves during the petrophysical evaluation in order to use porosity, water saturation, and permeability data in the new technological applications.

Rock type

Knowing the types of rocks allows us to:

Differentiate the flow units, permeability units.
Classify the reservoirs and petrochemical properties.
Understand the different pore structures.

Determining a rock type means that we know a specific geometry. To determine the rock type we use the Winland Equation (1972) which is an empirical relationship between porosity, air permeability and pore throat corresponding to a mercury saturation of 35% (R35). The Winland equation was used and published by Kolodzie (1980) and is given below:

Log R 35 =0.732 + 0.588(k)-0.864Log (Φ)

Where R35 is the pore throat radius (microns) corresponding to the 35th percentile, k air is the uncorrected air permeability (md), and φ is porosity (%).

From this equation, calculation was made to determine the rock types and to estimate the pore throat size for each of them. Assuming that the rock type may be expressed mathematically, with ø and k as its necessary components, through this relation is a better understanding of the facies. After the calculations and petrophysical evaluation with conventional logs and calibration with core data were made, we identified 4 different quality rock types, as shown in Figure 14. They range from rock type 1 with 2000 to 3800 mD permeability to the rock type 4, with 0.8 to 40 mD. The Table in the Figure 15 also shows the values of the basic parameters for each rock type. Figure 16 shows the percentages of each rock type in Ejm 7 reservoir.

Flow Units and Lorenz Graphic Application

The detailed description of the pore geometry constitutes an equally fundamental aspect of the petrophysical characterization. The basis for determination of flow units in the reservoir is based in the analysis of pore throats and the relation of porosity and permeability.

The flow unit is the volume of rock that shows similar geological and petrophysical properties, which, in turn, are clearly different from other rock volumes. This concept is widely used in core analysis (Ohen and Austin, 2003). This concept modifies the traditional way of evaluating a reservoir. Previously, the reservoir was considered to have isotropic and homogeneous properties; however, the heterogeneous and varying characteristics of the reservoir have been noted in studies performed during the 1990s (Ohen and Austin, 2003; Gunter and Viro, 2006). This heterogeneous system consists of multiple homogeneous and non-uniform subgroups, which have been named flow units. The flow unit, as a rock unit inside the reservoir, can be plotted; its porosity and permeability define the distribution and flow of fluids (Gunter and Viro, 2006). Pore-throat size and the Lorenz cross plot are taken into account in the definition of the flow units. It allows us to determine the flow units in reservoir, based on the flow capability and capacity of storage (Figure 17). Nine flow units were recognized***;*** this has allowed us to determine barriers and the best zones of flow in the reservoir.

Flow Zone Indicator

The Flow Zone Indicator (FZI) is another basic parameter used to identify the majority of geologic variables that control the flow of fluids. The flow unit with the highest FZI has the largest relationship between the pore throats, and can be expressed as follows:

FZI = RQI / PHIZ

The FZI value is, therefore, a unique, homogeneous, and non-uniform property for each flow unit. From laboratory tests, it has been determined that the value of FZI is a function of mineralogy and texture and that these parameters strongly affect the sensitivity of formation damage (Gunter and Viro, 2006).

PHIZ= Φz= (Φ/ 1-Φ)

The Rock Quality Index (RQI) links microscopic attributes of the pore space with petrophysical parameters of the reservoir (Figure 18). Furthermore, RQI is a close approximation of the average hydraulic radii (pore throat) present in the reservoir; it should be noted that this observation was made using core analysis in the laboratory

RQI (microns) = 0.0314 $\sqrt{}$(K/ Φ)

Petrophysics Evaluation

Figure 17, which shows the porosity-thickness vs. production and permeability-thickness vs. production, represents the integrated

petrophysics evaluation and the production data for the Ejm7 reservoir. Displayed in Figure 19 are the conventional electric logs (GR, CALI, RT, NPHI, DPHI, shale volume (Vsh), effective porosity (PHIE), water saturation (Sw), pay zone, curve for different pore throats, R35 curve, FZI, RQI and the core calibration with computed curves.

Anisotropy

Anisotropy, which begins to develop during deposition and continues to develop further during diagenesis of the sediments, is measured by variation in shear wave velocity (Fogal and Kessler, 2002).

Sandstones develop anisotropic characteristics during deposition in response to the depositional process; in carbonates the predominant anisotropy is commonly generated by post-deposition events, such as fracturing.

The acoustic anisotropy in rocks can be characterized as intrinsic or induced by stresses (Jaeger and Cook, 1977). The intrinsic anisotropy exists in the absence of external stresses and can be caused by stratification, microstructures, or aligned fractures, whereas the anisotropy induced by stresses results from the tectonic stresses or overburden.

Data acquisition

A wave sonic is the tool used for the acquisition of information; it consists of the following components: transmitters and electronic control, acoustic isolator, sensors arrangement. This tool can select the frequency of the dipolar sources (Kessler, 2001).

The tool has three transmitters: a monopolar transmitter, omnidirectional, and two dipoles transmitters disposed orthogonally. The monopolar transmitter consists of a piezoelectric crystal designed to transmit the acoustic energy uniformly around the circumference of the tool with a central frequency of 5-6Khz and a bandwidth of 112 Khz. Using this frequency we obtain more investigation depth for compressional and shear waves refracted. We can get a complete waveform using the derivation of refracted arrivals.

The two dipolars sources (benders, bars), placed orthogonally, can control the flexural waves generation in X - X and Y-Y, with central frequency of 600 to2500 Hz. These low frequencies permit shear wave behavior to be obtained from the generation of flexural waves in the formation.

The acoustic isolator section allows the appropriate functioning of the tool; this element needs to be extremely flexible (to isolate the acoustic waves that travel in the surface of the tool), and it has to be strong (to allow operations with tubing and/or support the weight of other tools).

Arrangement of the receptors consists of 8 levels, spaced each 0.5 ft., every level with four sensors, two in line and the other two in cross-

line in the direction of the dipolar transmitters "X" and "Y". Sensors in line and cross line receive a total of 96 waveforms, 32 monopolar waveforms, 32 dipolar waveforms in the "X" axis, and 32 dipolar waveforms in the "Y" axis. The sensor frequency is 0.5 - 20 Khz.

The tool is oriented with a navigation package. This package is aligned with dipolar transmitter “X”, in order for to know the orientation of the events created by shear waves.

Processing and Results

To obtain the Delta-T value, a mathematical technique is used which correlates every sensor waveform and assigns a displacement interval that corresponds to a time period. The first waveform is compared with the second one (by the time and slowness that maximizes the coherence), and this is followed successively up to comparing all waveforms (32 in total), to give coherence or semblance, which can be quantified.

The anisotropy analysis implies a simultaneous solution of 64 wave forms produced by the shots of both dipolar transmitters “X” and “Y”; receiving every sensor waveform in line and crossed to determine:
Fast and slow shear velocity (transit time).
Fast shear velocity direction.
Waveform energy associated with both transmitter arrays in line and cross line.

The changes of energy in the crossed sensors are due to tool orientation changes. This effect is reduced when the sensor arrays are aligned by the fast or slow direction, but if they are positioned to 45° of those planes, this effect is maximized.

Applications

Because the dipolar sonic was not run in B-35H, these logs were acquired in a nearby well, “B-33”, with similarity in development of the zones (Figure 20). The wells are 673 m apart.

Study of the B-35H core shows that the maximum stress has a NNW-SSE to N-S preferential direction (Figure 21). This interpretation was corroborated by the dipolar sonic tool data from B-33 well (Figure 22). Figure 23 shows the correlation between Young’s modulus from sidewall cores in B-35H and that derived from wellbore stability processing for B-33.

Discussion

If we use the results of the petrophysical evaluation, it is possible to predict the seismic response at locations in the field during development and to interpret the observed anomalies.

The petrophysics and the petrography, including the SEM analysis, are tools to determine how the mineralogy and the fabric interact with the fluids. Accuracy of petrophysics is important for the description of the elastic properties. Both are complementary in reservoir characterization.

Conclusions

1.- Rock properties were calibrated for the Ejm7 reservoir;
Petrophysical characteristics (porosity "ø", water saturation “Sw”, permeability k, mineralogy, texture, and NaCl (Rw)) resulted in recognition of:

- 4 Types of rock.
- 9 units of flow.

2.-The principal variables of the unit of flow are the indicator of flow (FZI), the index of rock quality (RQI), and the value R35.
3.-The petrochemical data and core images show that the Ejm7 reservoir presents excellent conditions to store and yield hydrocarbons.
4.-The rock types and flow units provide a more detailed understanding of the reservoir and support its characterization.
5.- Data integration and new methodologies are used to get a better understanding of the reservoir.
6.- Results support the sedimentary and petrophysical models made.
7.- It is suggested that additional sidewall cores in the pay zone will result in a better understanding of the reservoir geomechanics, which can be used to avoid fines (sediment) production and to determine the critical flow pressure without damaging the formation
8.- The maximum stress has a N-S preferential direction, this is confirmation of the determination by the anisotropic cross dipolar sonic tool.

Acknowledgements

The authors give thanks to PEMEX Exploration and Production (PEP) for permission to publish this document.

Also we want to express our gratitude to the members of the multidisciplinary team Comitas – Torrecillas, for the facility to use the information. The authors too give thanks to Cristina Aguilera T. for her help in the translation of his paper.

References

Alzaga, Ruiz H., and Estavillo Gonzalez C., 1993, Curso: Estratigrafía y sedimentología de terrígenos: CAD-1105IMP.

Avalos Torres, H., et al., 2007, Estudio Geológico y Petrofísico del Yacimiento Ov-c50 del Campo Cañón, Cuenca de Burgos: 2do. Congreso y Exposición Internacional del Petróleo en México. Veracruz, México. 28-30 June 2007.

Avalos Torres, H., et al., 2008, Geology and petrophysic of a reservoir from Cañón field, Burgos basin, México: AAPG Annual Convention and Exhibition. San Antonio, Texas. 20 - 23 April 2008.

Avalos Torres, H., et al., 2009, Estudio y Subdivisión Petrofísica del Yacimiento Ejm7 en el pozo horizontal Bayo35; Área Comitas – Torrecillas: Jornadas Técnicas AMGP. ReynosTamaulipas, México. 13 February 2009.

Carranza-Edwards Arturo. 1980, Ambientes Sedimentarios Recientes de la LlanuCostera Sur del Itsmo de Tehuantepec: Anales del Centro de Ciencias del Mar y Limnologia. Contribución 113. UNAM.

Core Lab, 2001 and 2008. Reportes final de núcleos (convencional y depared) de los pozos Numerador-1, Bayo- y Bayo-35H: Petrofísica Básica y Especial; Análisis Petrográfico, Microscopio Electrónicde Barrido y Sedimentológico": Propiedad de PEMEX Exploración y Producción.

Hurlbut, Cornelius S., Jr., 1981, Manual de Mineralogía de Dana: 2ª Edición, Ed. Reventé. 653 p.. Echanove E., O., 1988, Geología Petrolera de la Cuenca deBurgos Asociación Mexicana de Geólogos Petroleros. Vol. XXVIII.

Fogal J,, and Kessler C., 2002, Application of shear anisotropy from a New Generation Crossed Dipole Acoustic Tool: 27th annual SPE.

Folk, R.L., 1974, Petrology of sedimentary rocks: Austin, Texas, Hemphill Publishing, 184 p.

Garrido, Ricardo, et al., 2009, Actualización en tiempo real del modelo estático, 3D del yacimiento Ejm7 campo Bayo, utilizando LWD en la perforación del pozo horizontal Bayo-35H: Congreso Mexicano del Petróleo 2009 Veracruz. Boca del Río, Veracruz, México. 11-13 Junio 2009.

Gunter, Gary, and Viro, José. E., 2006, Tipos de roca y unidades de flujo: NEXT. Curso de capacitación. Reynosa, México. Marzo 2006.

Gunter, Gary, et al., 1997, Overview of an integrated process model to develop petrophysical based reservoir description: SPE 38748.

Gomez R., Orlando, 1995, Curso de Evaluación de Registros Geofísicos Avanzados: AIPM, A.C. p. 304-312.

Halliburton, 1991, Open Hole Log Analysis and Formation Evaluation. Chapter 17-18.
Granados H., Juan C., 2003, Caracterización petrofísica de un yacimiento de la cuenca de Burgos: Rev. El Fronterizo AMGP. v. 3. n. 1, p. 20-24.

Jaeger, J.C., and N. G. W. Cook, 1979, Fundamentals of Rock Mechanics, 3rd edition: Chapman and Hall, London. . Methuen, London, 1969.

Kessler, C., 2001, A new Generation Cross Dipole Logging tool; designs and case Histories: SPE 71740. Rider, Malcolm, 1999, The Geological Interpretation of Well Logs: second edition. Gulf Publishing Company.

LaFage, Stéphanie, 2008, An Alternative to the Winland R35 Method for Determining Carbonate Reservoir Quality: Thesis. Texas A&M University.

Linares, R. Hugo, 2003, Unidades de flujo. Principios y aplicación en pozos de los campos Corindón y Pandura: Rev. El Fronterizo AMGP. v. 3. n. 3, p. 23-30.

Ohen H., and Austin, A. Caracterizando y multiplicando el modelo geológico para el modelado mecánico: Core Lab. Curso de capacitación. Reynosa, México. Febrero 2003.

Tarbuck and Lutgens, 2004, Ciencias de la tierra: Ed. Pearson-Prentice Hall, p.29-51 and 131-144. Winkler, K., Sinha, B., and Plona, J., 1998, Effects of Borehole Stress concentrations on dipole anisotropy measurements: Geophysics, v. 63, n. 1, (January-February 1998); p. 11.

Glossary

BVI Bulk Volume Irreducible
CNL Compensated Neutron Log
CSNG Gamma Ray spectroscopy
D Darcy (permeability unit)
DPHI Density porosity
Ejm7 Eocene Jackson medium (middle) - 7
FZI Flow Zone Index
GR Gamma Ray Log
Gr/cc Grams per cubic centimeter
HRI High Resolution Induction
IH Hydrogen Index
Khz Kilohertz (unidad de frecuencia) k Permeability
LDL Litho density Log
mD Millidarcy (permeability unit)

MD Measured depth
Mmpfd Million cubic feet per day
NaCl Sodium chloride
NPHI Neutron porosity
Ppm Parts per million
PAY Pay zone
PHIE effective porosity
PHIZ Zone porosity
Qc Condensate rate
Qg Gas rate
R35 35% Ratio Hg Saturation
RHOB Bulk density
RQI Rock Quality Index
Rt True Resistivity
Rw Water resistivity
SEM Scannng Electronic Microscope
Sw Water Saturation
Vsh Shale volume
WS Wave Sonic Log
Psi Pressure unit
Qg Gas rate
TVD True Vertical Depth
Φ Porosity

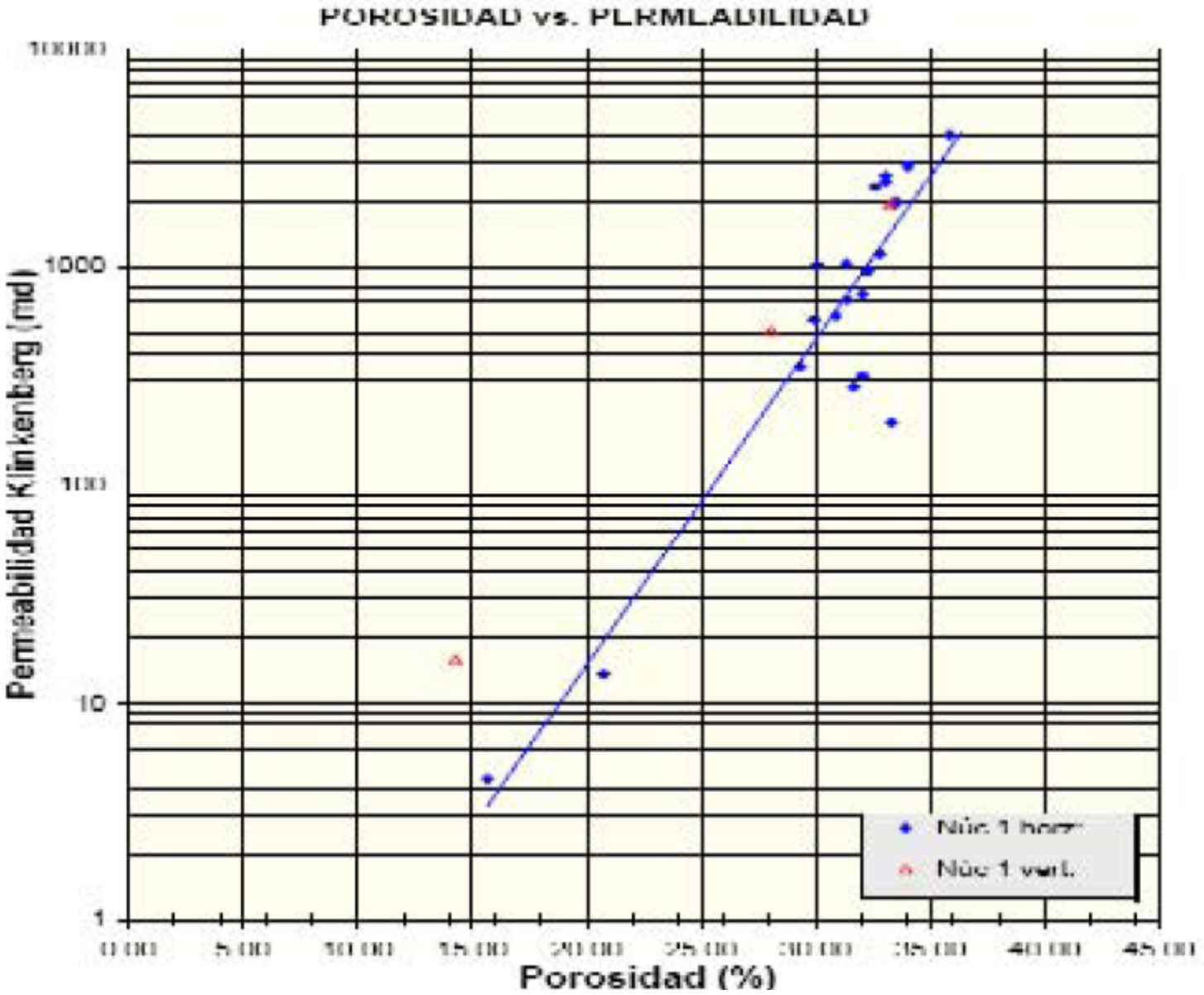

Figure 13. Porosity vs permeability, in B-35H; ø= 15-35%; k=4-4000 mD. (Core Lab, 2008).

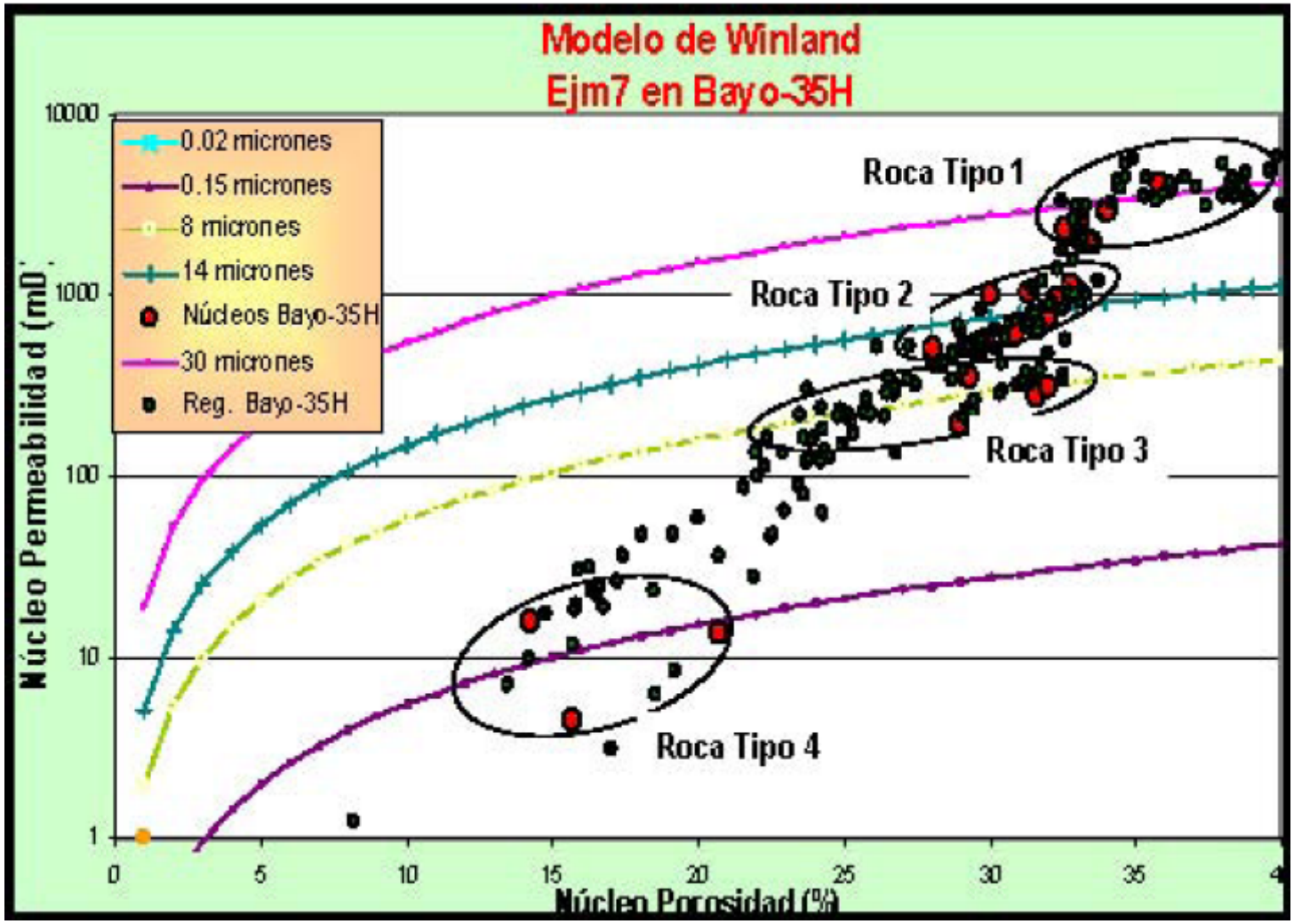

Figure 14--Plots of the four rock types in Ejm 7 reservoir, as delineated by the Winland equation, from core data and petrochemical evaluation, based on pore-throat size.

Tipos Roca	%RT	H	K (mD)	PHI (%)
Tipo Roca 1	0.33	11.00	954.4755	32.44
Tipo Roca 2	0.29	9.50	222.7528	27.82
Tipo Roca 3	0.27	8.88	11.1684	17.53
Tipo Roca 4	0.11	3.50	0.0420	6.81

Figure 15. Porosity (PHIE), permeability (k), and thickness (H) values.

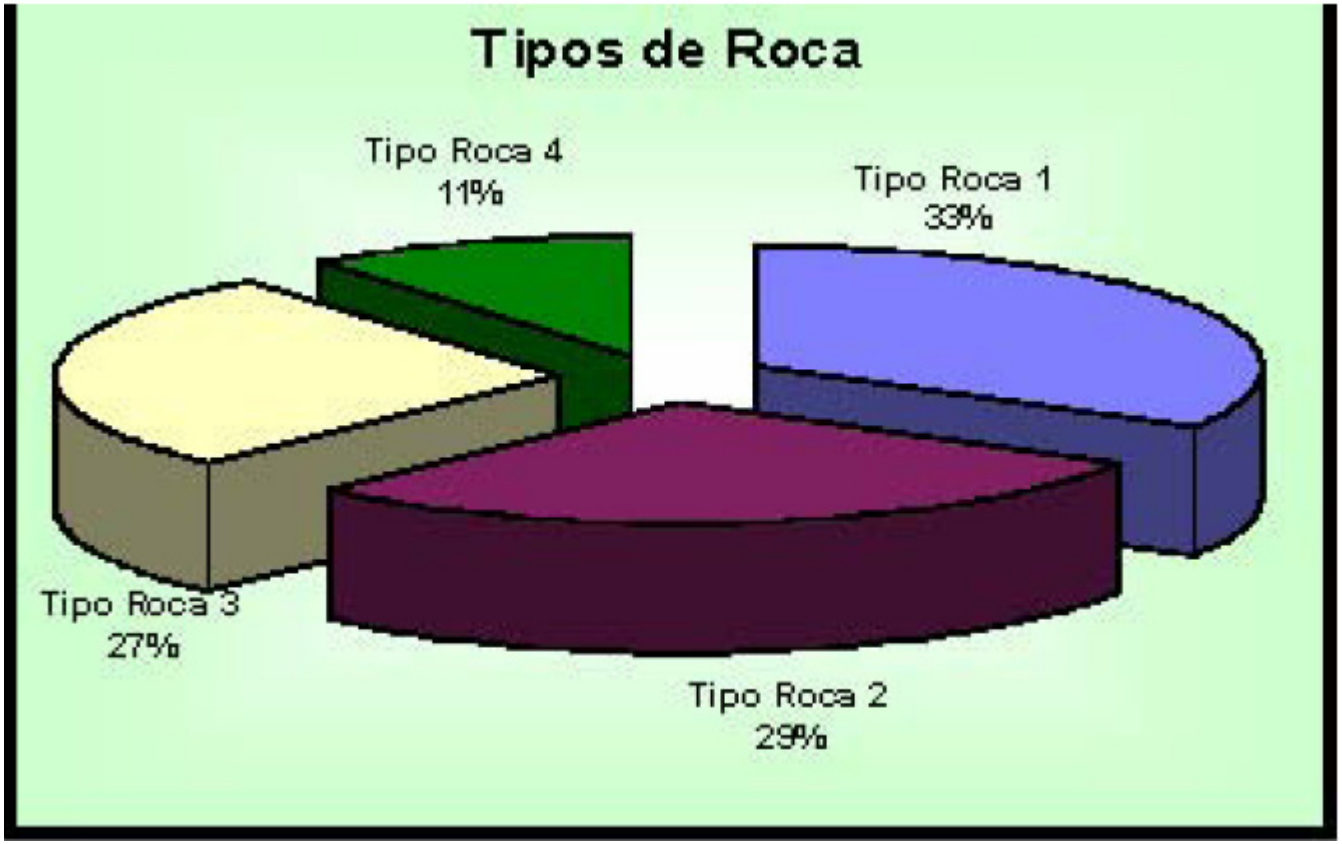

Figure 16--Pie diagram showing different percentages of the four rock types in Ejm 7 reservoir.

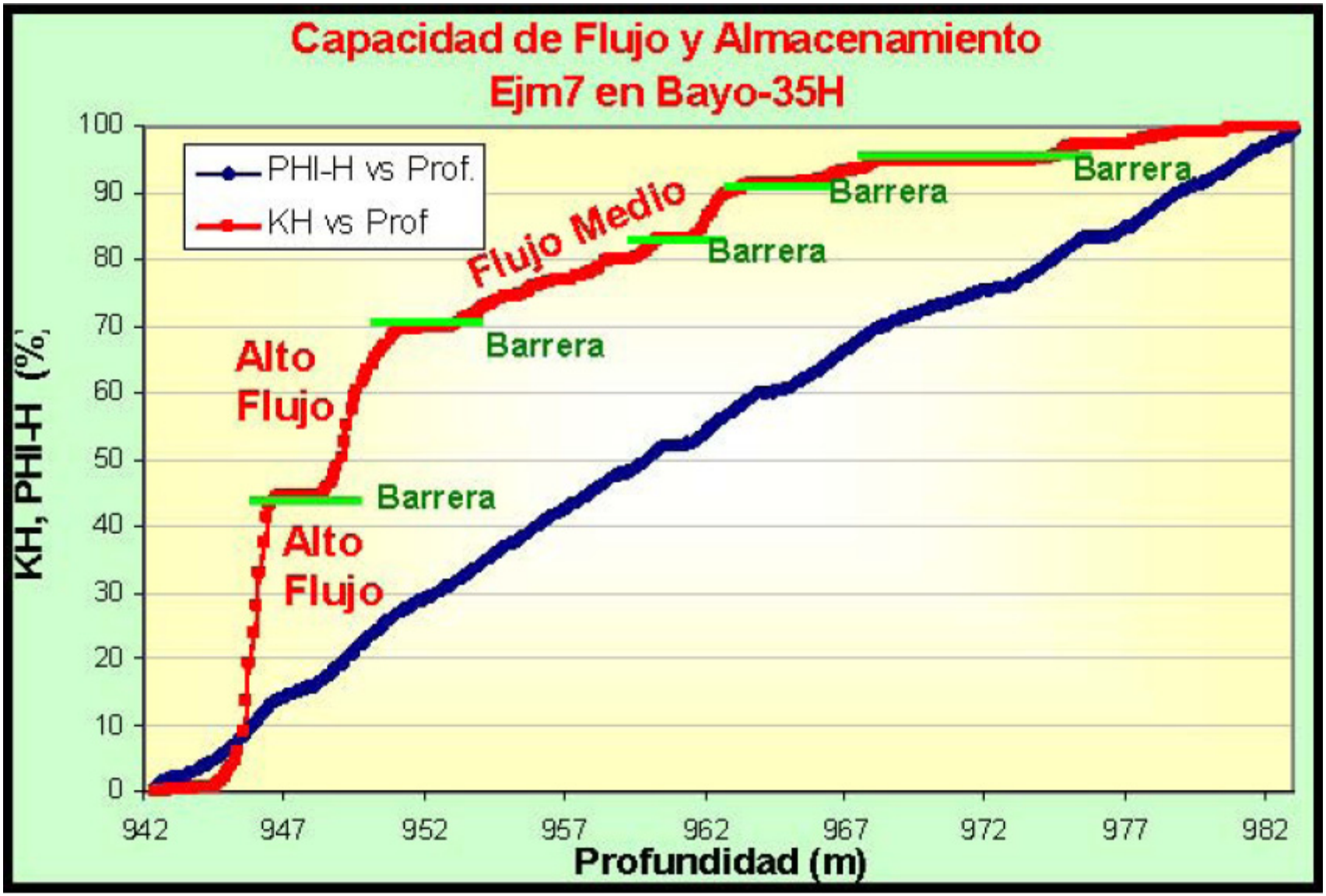

Figure 17. Graph of flow capability (KH/PHIH) vs. storage capacity with respect to depth of Ejm 7 in B35-H well.

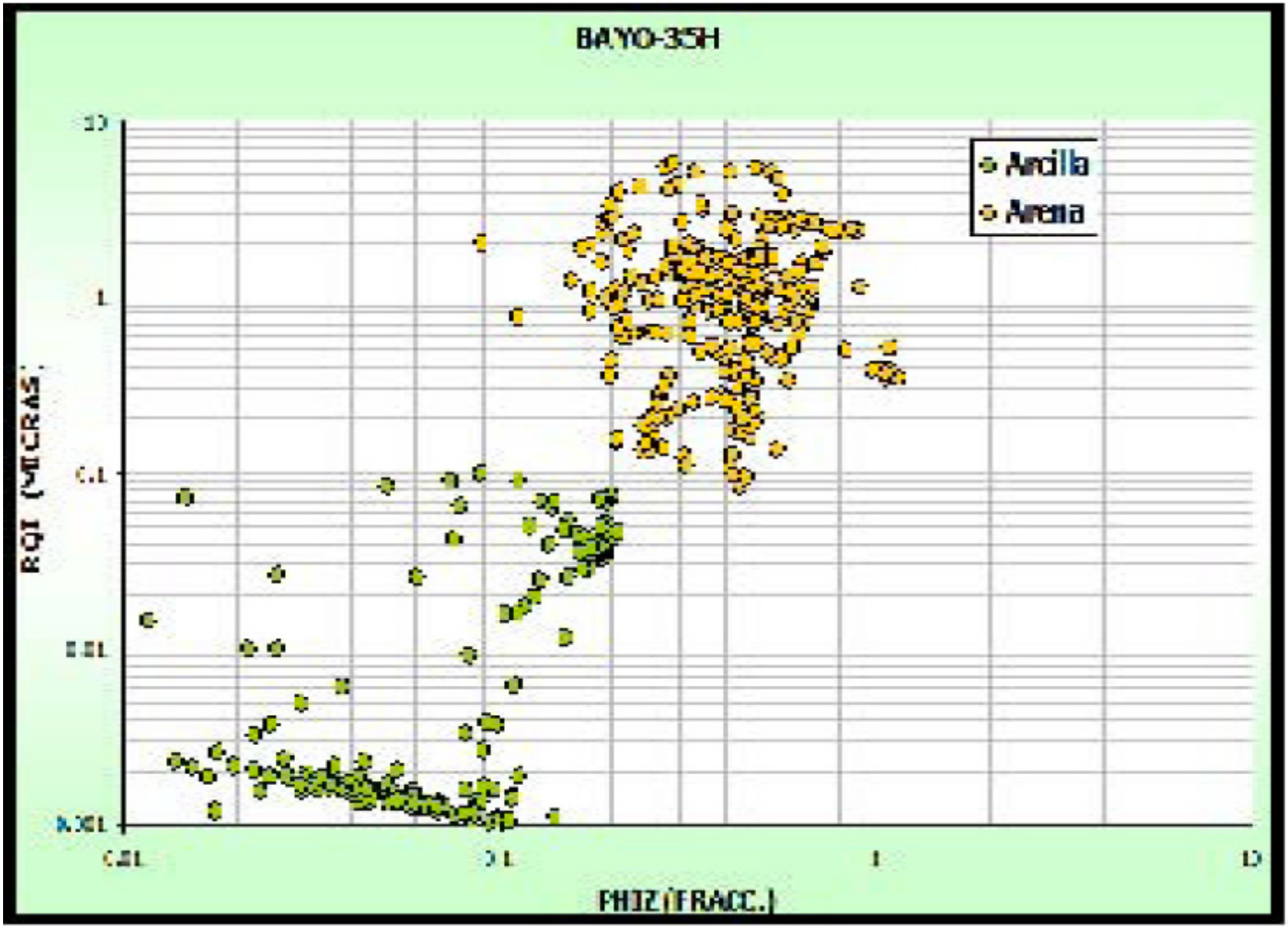

Figure 18. Cross plots of RQI vs PHIZ in Ejm7 reservoir.

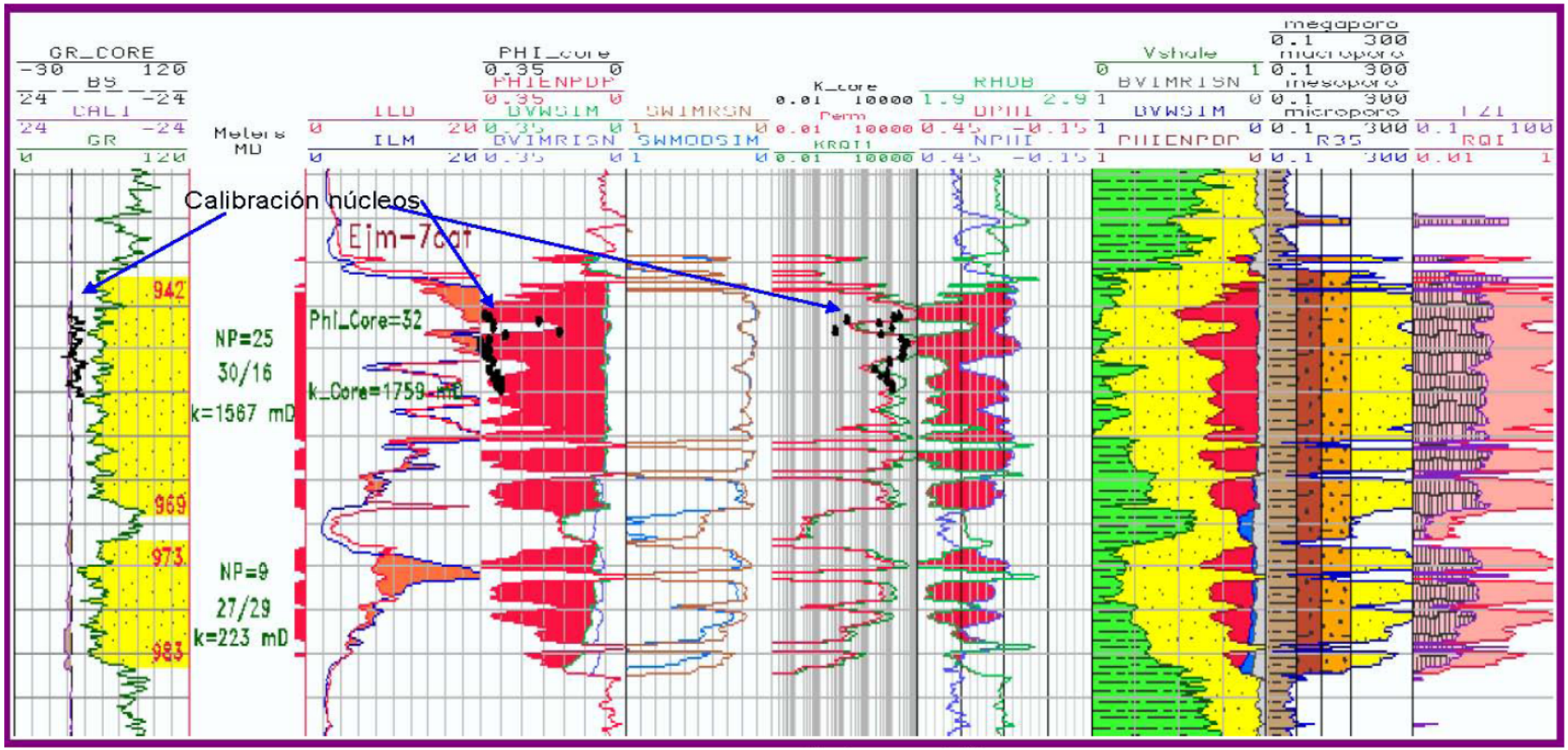

Figure 19. Petrophysical evaluation of Ejm 7 reservoir.

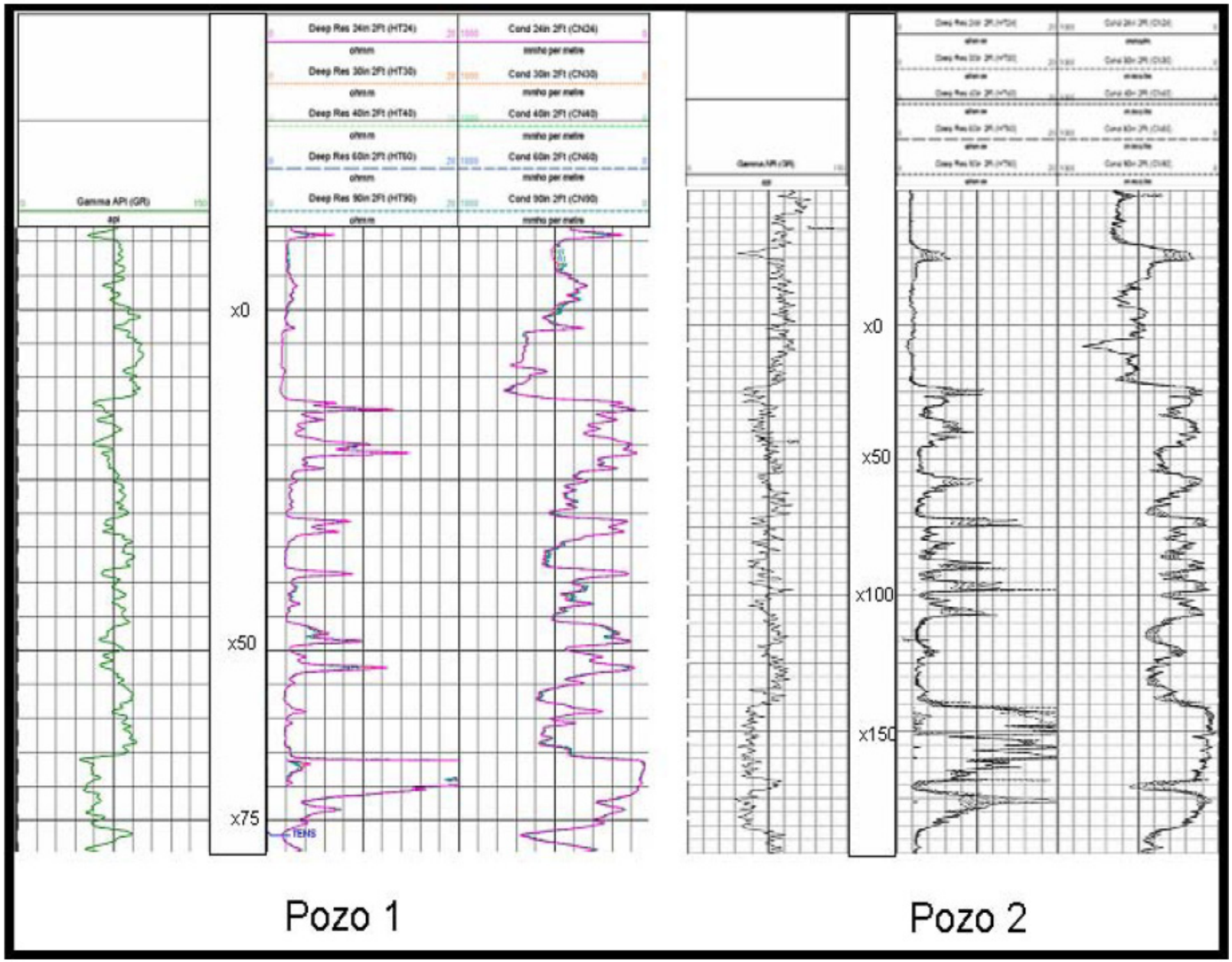

Figure 20. Logs of equivalent stratigraphic section in wells B-35H and B-33.

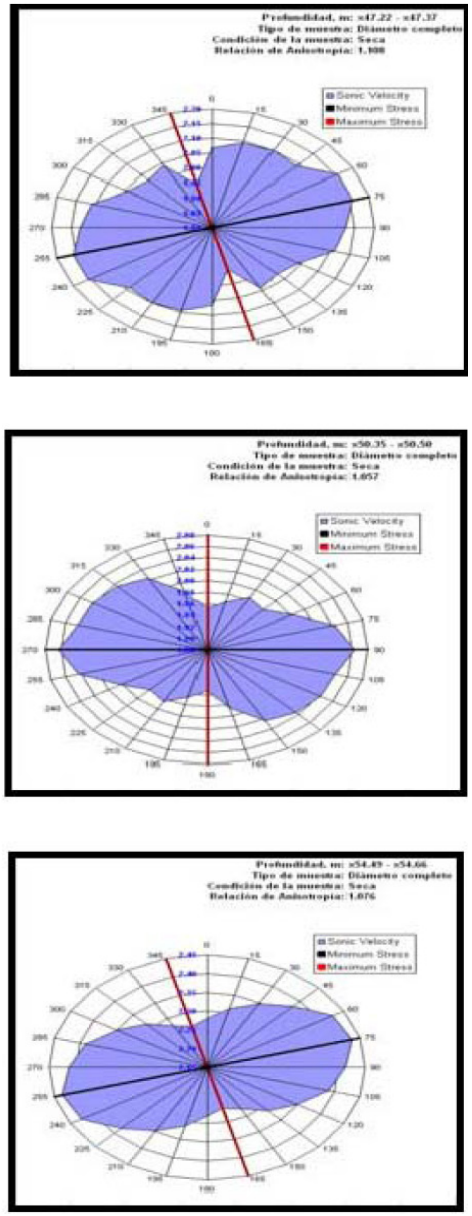

Figure 21. Schmidt diagrams showing results of anisotropic acoustic velocity from three core samples in well B-35H. Maximum stress direction is approximately N-S.

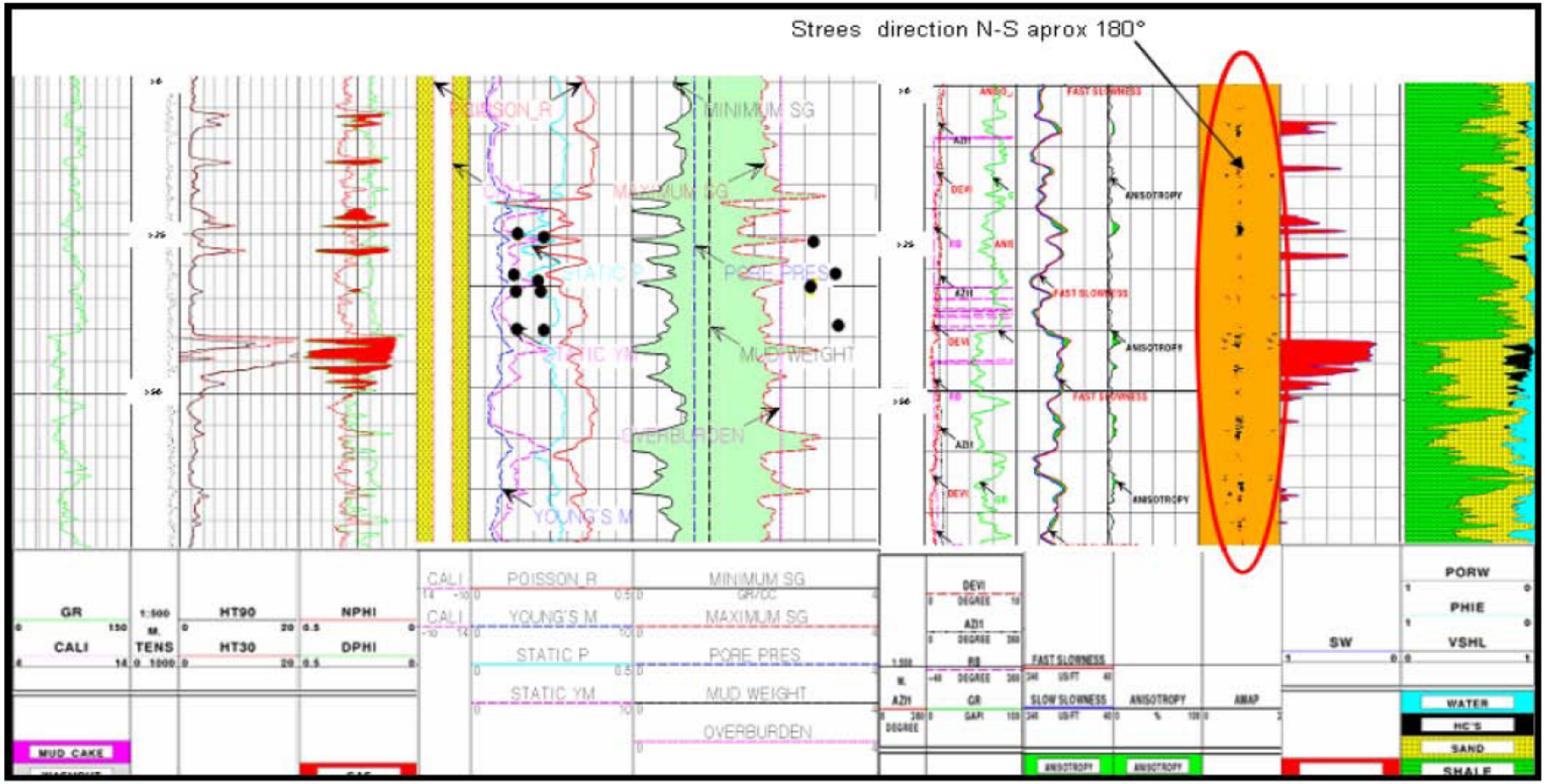

Figure 22. Preferential N-S direction is highlighted on the anisotropy process log.

\

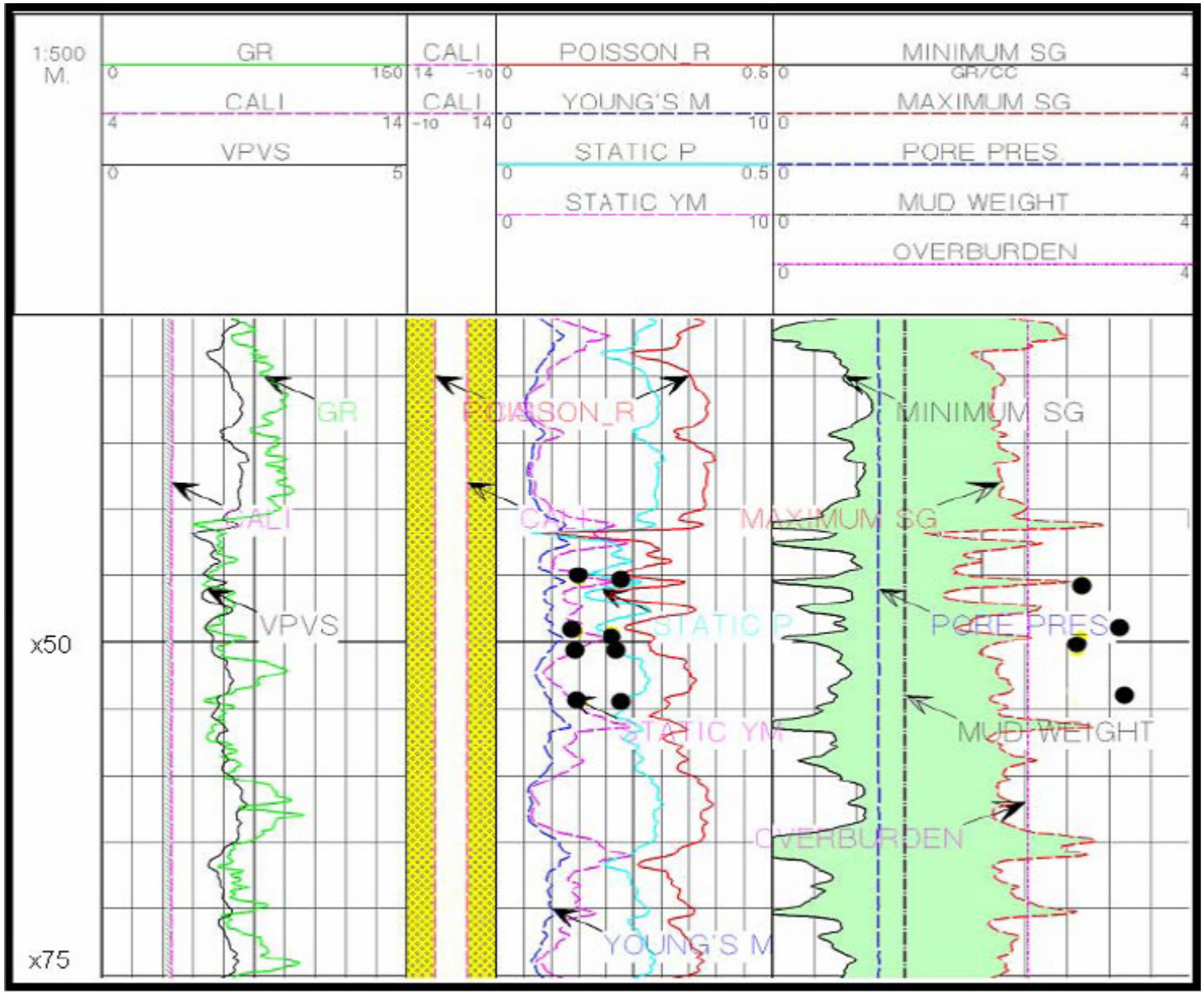

Figure 23. Wellbore stability process (Young's modulus and Poisson's ratio) in B-33 well.